Structural, optical and magnetic properties of Ni-aluminates with Co substitution

M.E. Gouda [a,*], W.A.A. Bayoumy [b]

[a] Physics Department, Faculty of Science, Benha University, Banha, Egypt

[b] Chemistry Department, Faculty of Science, Benha University, Benha, Egypt

Abstract— Nickel – Cobalt aluminates nanoparticles (NPs) in the range of 3-27 nm were synthesized by a sol-gel auto combustion method using citric acid as fuel. The as-synthesized (NPs) have been characterized by X-ray diffraction (XRD), Fourier transform infrared spectroscopy (FT-IR), Brunauer Emmett Teller (BET) surface area analysis, **v**ibrating sample magnetometer (VSM), UV–Vis spectroscopy and CIE-L*a*b* color measurement. Formation of spinel phase was identified by XRD. Cationic distributions for the present investigated system were estimated. The colorimetric data pointed out to the formation of blue pigments. These (NPs) exhibit a superparamagnetic behavior at room temperature with no coercivity and remanence.

Keywords — Ceramic pigments; Cationic distribution; Nanoparticles; Optical properties; Superparamagnetic.

1 INTRODUCTION

In recent years there has been increasing interest in the synthesis of nanocrystalline spinel aluminates with the general formula MAl_2O_4 (M=Ni, Co, Mg and Cu….etc). Generally aluminates spinels have high thermal stability, high mechanical resistance, hydrophobicity, and low surface acidity [1]; justifying its widespread use in many applications; Most importantly their application as including refractory materials with high melting temperatures, catalytic materials , ceramic pigment, gases sensor, magnetic materials, color TV tubes and solar absorber [2-7]. Several preparation methods have been used to obtain crystalline aluminate spinels with small particle size, such as hydrothermal [8], solid-state reaction [9], mechano-chemical synthesis [10], and sol-gel [11].

It is well known that in the spinel structure AB_2O_4, the A and B cations occupy two different crystallographic sites, tetrahedral and octahedral. Occupation of tetrahedral sites by a divalent cation yields a normal spinel structure, while occupation of the octahedral sites by a divalent cation produces an inverse spinel structure [12]. If divalent cations are present on both A- and B-sites, the structure is mixed or disordered. The occupation between these two sites is affected by the combination and nature of the cations and depends on the processing conditions and impurity content. Nickel aluminate is typical for a partially inverse spinel in which Ni^{2+} and Al^{3+} ions are randomly located in both tetrahedral and octahedral positions, respectively [13,14]. Cation distribution studies have been used to improve the understanding of the correlation between the crystal structure and physical properties in aluminate spinels. Roelofsen et al., studied the variation in the cell edge, degree of inversion, positional parameter, and thermal parameters of $NiAl_2O_4$ at different temperatures between 800 and 1500 ℃ by Rietveld refinement using X-ray powder diffraction data [15]. Ianos and Barvinschi have prepared $Mg_{1-x}Ni_xAl_2O_4$ (x = 0, 0.25, 0.5, 0.75 and 1) by solution combustion technique [16]. All samples prepared had blue color shades, and exhibit spinel structure in which Ni^{2+} occupy each of tetrahedral and octahedral configurations. X-ray photospectroscopy (XPS) analyses on $CoAl_2O_4$ nanocrystals showed that the Al^{3+} and Co^{2+} ions occupy both octahedral and tetrahedral sites in spinel structure [17]. To our knowledge, structural studies and effect of citric acid as fuel on phase formation and size of $NiAl_2O_4$ and transition metal Co doped $NiAl_2O_4$ are not abundant in the literature. Therefore, based on the above rationale, our research is set out to prepare and characterize $Ni_{1-x}Co_xAl_2O_4$ (x =0, 0.2, 0.4, 0.6, 0.8 and 1) spinel pigment by modification combustion method in presence of citric acid as a fuel. The structural location of Co^{2+} , Ni^{2+} and Al^{3+} in the $Ni_{1-x}Co_xAl_2O_4$ spinel structure have been proposed on the basis of XRD data analysis, magnetic and optical properties.

2 EXPERIMENTAL

2.1 Materials

All the chemical reagents used in the preparation were A.R. grade and used without further purification and treatment. All materials: cobalt nitrate ($Co(NO_3)_2 \cdot 6H_2O$), aluminum nitrate ($Al(NO_3)_3 \cdot 9H_2O$), nickel nitrate ($Ni(NO_3)_2 \cdot 6H_2O$), polyethylene glycol (PEG) and citric acid are supplied from Adwic, except cetyltrimethyl ammonium bromide monohydrate (CTAB) {$CH_3(CH_2)_{15}N(CH_3)_3Br$} is provided from Aldrich.

• *Corresponding auther: M.E. Gouda*
E-mail address: migouda88@gmail.com

2.2 Synthesis

$Ni_{1-x}Co_xAl_2O_4$ nanoparticles with the composition of (x = 0.0, 0.2, 0.4, 0.6, 0.8 and 1.0) were prepared by a combination of hydrothermal and combustion methods in which Cetyl Trimethyl Ammonium Bromide (CTAB) surfactant and polyethylene glycol (PEG) are used as structure directing agents and citric acid as a fuel and a chelating agent. Stoichiometric amounts of cobalt nitrate ($Co(NO_3)_2.6H_2O$), nickel nitrate ($Ni(NO_3)_2\cdot 6H_2O$) and aluminum nitrate ($Al(NO_3)_3.9H_2O$) as cation sources were dissolved in distilled water. Then proper amount of citric acid, CTAB and PEG was added to the above solution with stirring. The molar ratio of metal ions: citric acid: CTAB: PEG was (1: 2: 4.44: 8.88). The mixed solution was stirred for 3 h at 80 ℃ until a highly viscous gel was formed. The pink gels were dried in oven at 100 ℃ and then calcined at 600 ℃ for 2 h. The prepared $Ni_{1-x}Co_xAl_2O_4$ spinel with different molar ratios of cobalt 0.0, 0.2, 0.4, 0.6, 0.8 and 1.0 were labeled as C0.0, C0.2, C0.4, C0.6, C0.8 and C1.0, respectively.

2.3 Characterization

The phase composition of the powders was investigated by (XRD) using a model Philips PW-3710 diffractometer with Cu Kα radiation in a 2θ range from10° to 80°. FT-IR spectroscopic analysis using KBr pellets was carried out using a Brucker-FTIR spectrometer. The magnetic property was measured using VSM-9600M at room temperature with an applied magnetic field of 15 kOe. The specific surface area of the powders was studied by BET nitrogen gas adsorption technique using a BET volumetric apparatus. The diffuse reflectance and the chromatic CIE-L*a*b* of the studied samples were measured in JASCO spectrophotometer UV–visible in 200–800 nm range using standard D65 illumination and barium sulfate as a reference material [18]. L*a*b* are chromatic parameters used in order to allow everyone to simulate the corresponding coloration with common drawing software.

3 Results and Discussion

3.1 X-ray diffraction

The XRD spectrum of $Ni_{1-x}Co_xAl_2O_4$ (x = 0.0, 0.2, 0.4, 0.6, 0.8 and 1.0) samples calcined at 600 °C is shown in Fig. 1. The main peaks are indexed in accordance with spinel structures (ICDD file 82-2252 and PDF file 10-0339 for C1.0 and C0.0, respectively). For the samples C0.0 and C0.2 a small proportion of the NiO phase (ICDD 78-0643) is present beside the spinel phase. On other hand, XRD patterns showed formation of single phase in the samples (C0.4- C1.0), except the samples (C0.0 and C0.2) which are constituted traces of NiO. To investigate the effect of sintering temperature on the phases formed in (C0.0), XRD of the sample sintered at three temperatures (800, 1000 and 1100 °C) for 2 h was investigated. The results, Fig. 2, showed that NiO phase did not disappear with increasing sintering temperature, which agrees with that found by Han [19].

For spinel structure, the lattice parameter (a) can be calculated using the following relation [20]:

$$a = d\,(h^2 + k^2 + l^2)^{0.5} \qquad (1)$$

where (h k l) are the Miller indices and (d) is the inter-planar spacing. By plotting the value of $(h^2 + k^2 + l^2)$ versus $1/d^2$, the values of the lattice constant (a) was determined for each sample and listed in Table 1.

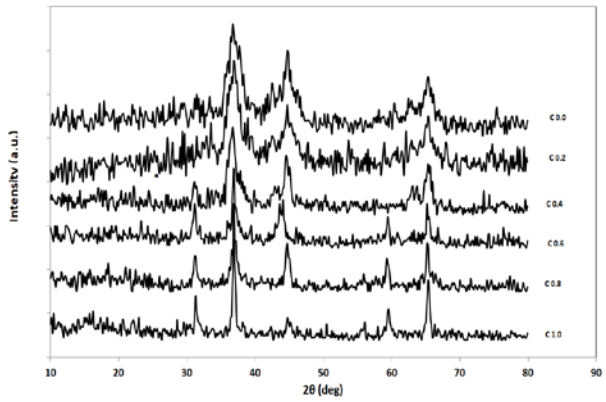

Fig. 1 X-ray diffraction pattern of $Ni_{1-x}Co_xAl_2O_4$ nanoparticles annealed at 600 °C.

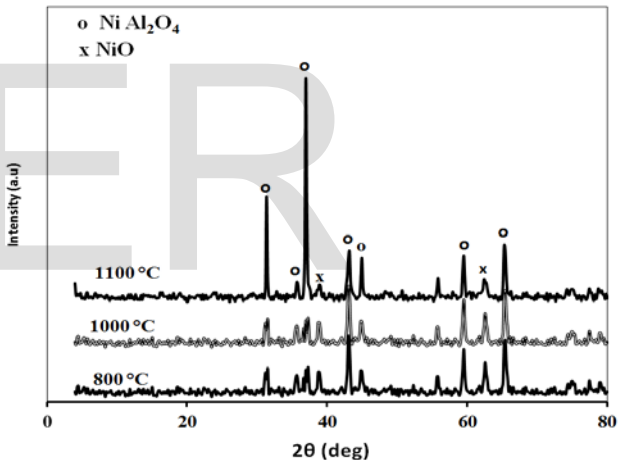

Fig. 2 X-ray diffraction patterns of $NiAl_2O_4$ nanoparticles (C0.0) annealed at different temperatures.

The lattice parameter was found to be changing in the range of that of C0.0 (8.0094 Å) and C1.0 (8.0998 Å). The increase in lattice parameter with Co^{2+} content can be explained on the basis of difference in ionic radii of Ni^{2+} and Co^{2+}. The larger ionic radius of Co^{2+} (0.745 Å) replaced the smaller ionic radius of Ni^{2+} (0.69 Å), consequently the lattice parameter increased due to an expansion in the unit cell. The average crystallite sizes (L) for the investigated samples were calculated from the (311) peaks according to Scherrer's equation [21]:

$$L = 0.89\,\lambda / \beta \cos\theta \qquad (2)$$

where, λ, the x-ray wave length, θ, the diffraction angle and β, the full-width at the half maximum of the observed peaks.The values obtained are listed in (Table 1). The crystallite sizes lie in the range of 3-27 nm, evidencing the nanometer character of

the samples. The crystallites sizes also illustrate increase with Co^{2+} content. The X-ray density of all the compositions was calculated using the formula [21]:

$$D_{XRD} = ZM/Na^3 \qquad (3)$$

where Z is the number of molecular unit cell Z=8; M is the molecular weight; N is the Avogadro's constant and a is the lattice parameter. The results obtained are also given in Table 1.

3.2 FT-IR spectroscopy

FT-IR spectra of the as-synthesized $Ni_{1-x}Co_xAl_2O_4$ nanoparticles taken in the 4000 – 400 cm-1 range is shown in Fig. 3. The spectra reveal absorption bands below 1000 cm^{-1} which are typical of AB_2O_4 spinel. The main absorption bands are listed in Table 1.The FT-IR vibrational frequencies depend on the cation mass, cation-oxygen bond length and the bond strength. The spectra for C0.0 show two bands at 760 and 510 cm^{-1} corresponding to tetrahedral Al-O stretching vibration and octahedral Ni-O stretching vibrations, respectively [22-24]. Whereas, the spectra of C1.0 show two bands at 660 and 545 cm^{-1} corresponding to tetrahedral CoO_4 and AlO_4 tetrahedral vibrations, respectively [25]. The intensity of CoO_4 tetrahedral band was found to increase with increasing the Co^{2+} content in the sample referring to the increase in Co-occupation of the tetrahedral sites with increasing x in the $Ni_{1-x}Co_xAl_2O_4$ samples.

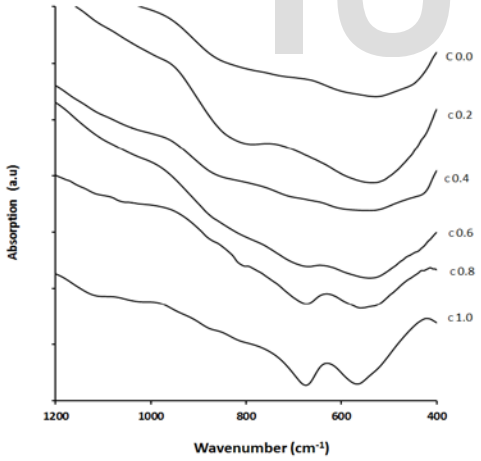

Fig. 3 FT-IR pattern of as-synthesized $Ni_{1-x}Co_xAl_2O_4$ nanoparticles.

3.3 Surface properties

The effect of composition on the surface properties and textural features of the studied system were investigated using BET technique. Fig. 4 shows typical plots for the N_2 adsorption/desorption isotherms for C0.0, C0.4 and C1.0 samples. In terms of the shape, the isotherms of all the samples, except C0.0, were found to belong to the type IV with the

Table 1: Lattice parameter (a), average crystallite sizes (L), X-ray densities (D_x), FT-IR spectral data (ν_1 , ν_2), surface area, porevolume and pore diameter of $Ni_{1-x}Co_xAl_2O_4$ samples.

Sample	a Å	(L)nm	(D_x) g.cm^{-3}	ν_1 cm^{-1}	$\nu_2$cm^{-1}	SurfaceArea (m^2/g)	Pore volume (ml/g)	Pore radius (nm)
C0.0	8.0094	3	4.567	760	510	56.0	0.09	4.11
C0.2	8.0381	4	4.519	752	513	23.0	0.11	11.81
C0.4	8.0501	5	4.500	760	517	41.0	0.19	11.85
C0.6	8.0701	7	4.468	650	521	26.0	0.10	9.75
C0.8	8.0813	16	4.451	654	522	25.0	0.12	12.04
C1.0	8.0998	27	4.422	660	545	24.8	0.06	5.76

H2 hysteresis according to the (IUPAC) classification. Such isotherms indicate the formation of a mesoporous structure [26] with inner bottle like pores. The isotherm of C0.0 sample, Fig. 4, shows the type II with the H4 hysteresis, which is often associated with narrow slit-like pores. The data obtained are summarized and listed in Table 1. From which it can be seen that the surface area decreases as the particle size increases and Co-content increases. Also, the results obtained for C0.0 refer to a great possibility to can be used as a catalytic support material.

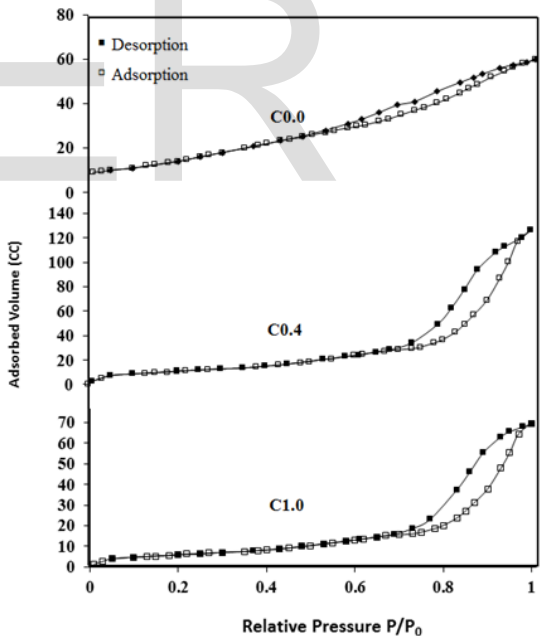

Fig. 4 Nitrogen Adsorption- desorption isotherms of $Ni_{1-x}Co_xAl_2O_4$ nanoparticles (C0.0, C0.4 and C1.0 samples).

3.4 UV–Vis spectroscopy and color characterization

Optical absorption properties of the $Ni_xCo_{1-x}Al_2O_4$ nanoparticles prepared at 600°C were investigated at room temperature by UV–Vis spectroscopy. Fig. 5 shows the absorbance spectrum of sample (C1.0) with four absorption bands in 250 - 350,

400 - 530, 550 - 570 and 650 - 800 nm wavelength ranges. The first band can be assigned to the $O^{2-} \rightarrow Co^{2+}$ charge transfer process while the second one to the $O^{2-} \rightarrow Co^{3+}$ charge transfer [27]. The energy-level diagram for Co^{2+} ($3d^7$ configurations) in

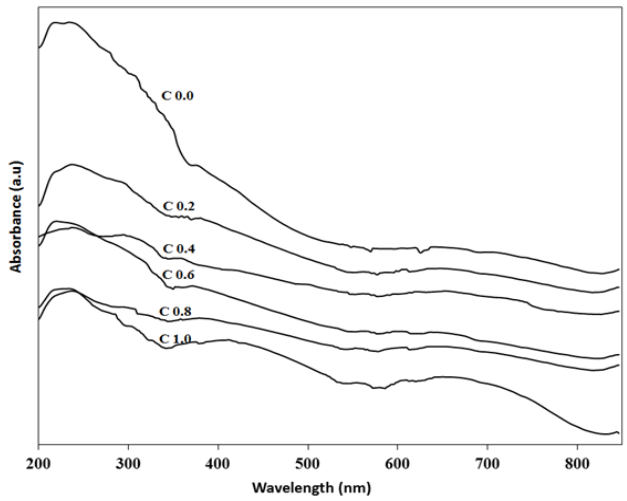

Fig. 5 UV-vis absorbance spectra of as-synthesized $Ni_{1-x}Co_xAl_2O_4$ nanoparticles annealed at 600 °C.

both octahedral and tetrahedral ligand fields, presents three spin-allowed transitions. Regarding Co^{2+} in a tetrahedral ligand field, it was detected a triple band ascribed to the [$^4A_2$ (F) → $^4T_1$ (P)] transition at around ~ 650 nm (red region), 550 nm (yellow-orange region), and ~ 530 nm (green region), which gives rise to the blue coloration. This triple band can be attributed to a Jahn-Teller distortion of the tetrahedral structure [28].The band observed at 250-350 nm is assigned to $^4T_1(F) \rightarrow {}^4T_1$ (P) transition for Co^{2+} ions in octahedral ligand field [29].

The absorbance spectrum for (C0.0) is also given in Fig. 4. It shows four absorption bands at 240-355, 360-555, 580-620 and 630 -800 nm. According to the literature [30,31], the absorption band at 580 – 620 nm is corresponding to the electronic transition $^3T_1(F) \rightarrow {}^3T_1(p)$assigned to tetrahedrally coordinated Ni^{2+}, the band at 630 -800 is due to transition $^3A_{2g}(F) \rightarrow {}^3T_{1g}$ (F) assigned to octahedrally coordinated Ni^{2+} and the bands at 240-355 and 360-555 are assigned to the charge transfer. According to the presence of different site geometry for C0.2- C0.8 samples, so that for each transition we have several peaks. Further complexities arise from other electron transitions, like spin forbidden ones or vibration ionic transition in molecules. The intensity of the related absorption in these cases is however much lower than in spin allowed ones.

The optical band gap is determined using the following relation [32]:

$$(\alpha h\nu)^{1/n} = A\,(h\nu - E_g) \qquad (4)$$

where α, is the absorption coefficient, A, is constant, E_g, is the optical band gap of the material and the exponent (n) depends on the nature of electronic transition. The kind of transition is investigated by determining the power (n) that showed a value of n = ½ revealing to direct allowed transition. The E_g-value is calculated using the least square fitting of Eq. (4) and listed in Table 2.

The CIE-L*a*b* colorimetric coordinates (L* = 0 indicates black, L* = 100 indicates diffuse white; a* negative values indicate green and positive values indicate magenta; b* negative values indicate blue and positive values indicate yellow) [33]. The chromatic coordinates (L*, b* and a*) of the samples under study are displayed in Table 2. It can be seen that the lightness, L*, decreases with the increase of the Co content, pointing out the formation of darker colors. The coordinate a* was kept negative for all the samples, indicating a slight green contribution. In terms of the b* coordinate, it showed an intense blue color, that is confirmed by the large negative *b** values (from −7.7 to −13.1) for all the samples, with the tendency of showing the highest blue intensity for the medium level of Co content, but leading to a blue color for all the samples.

Table 2 Lattice parameters (a, a_{th}), ionic radius (r_A, r_B), optical band gap (E_g) and color parameters (CIE-L*a*b*) of the $Ni_{1-x}Co_xAl_2O_4$ samples.

Sample	a (Å)		r (Å)		E_g, eV	L*	a*	b*
	a	a_{th}	r_A	r_B				
C0.0	8.0094	8.0192	0.5366	0.6153	3.4	71	-9.5	-7.7
C0.2	8.0381	8.0406	0.6157	0.5776	3.1	68	-7.9	-8.8
C0.4	8.0501	8.0560	0.6194	0.5813	3.6	66	-5.3	-10.2
C0.6	8.0701	8.0719	0.6251	0.5839	3.3	51	-4.2	-11.0
C0.8	8.0813	8.0879	0.6317	0.5862	3.5	43	-3.5	-12.1
C1.0	8.0998	8.0104	0.6379	0.5886	3.6	34	-2.3	-13.1

3.5 Estimation of the cation distribution

$Ni_{1-x}Co_xAl_2O_4$ spinel contains two types of sites: tetrahedral and octahedral sites. The distribution of the cations over these two sites can be expressed as:

$$(\,Ni_{\delta}\,Co_{\alpha}\,\,Al_{1-\delta-\alpha}\,)\,[\,Ni_{1-x-\delta}\,Co_{x-\alpha}\,Al_{1+\delta+\alpha}\,]O_4$$

Both the mean ionic radii of A-site (r_A) and B-site (r_B) can be calculated, using the cation distribution shown above, according to the present system as follows:

$$r_A = \delta\, r_{Ni} + \alpha\, r_{Co} + (1-\delta-\alpha)\, r_{Al} \qquad (5)$$

$$r_B = 1/2[(1-x-\delta)\, r_{Ni} + (x-\alpha)\, r_{Co} + (1+\delta+\alpha)\, r_{Al}] \qquad (6)$$

where *x* represents the level of incorporated Co^{2+} cations in the $NiAl_2O_4$ structure, *δ* and *a* are the concentration of Ni^{2+} and Co^{2+} ions, respectively, and r_{Ni} , r_{Co} , r_{Al} , are the ionic radii of Ni^{2+} (0.69 Å), Co^{2+} (0.745 Å) and Al^{3+} (0.535 Å), respectively. Using this formula the ionic radii of A-sites (r_A) and B-sites (r_B) were calculated and given in Table 2. The obtained tetrahedral (r_A) and octahedral (r_B) bond lengths were used to determine theoretically the lattice parameter of the spinel unit cell a_{th} using the equation [34]:

$$a_{th.} = (8/3\sqrt{3}) \quad [(r_A + R_o) + \sqrt{3}\,(r_B + R_o)] \qquad (7)$$

where R_o is the radius of the oxygen ion. The obtained values of the theoretical lattice parameter a_{th} are listed in Table 2. It can be seen that the calculated values a_{th} agree well with a that experimentally obtained from the XRD data.

3.6 Magnetic measurements

Fig. 6 shows typical plot for M-H curve for the as-prepared smple C1.0 at room temperature. It is observed from Fig. 6 that, saturation magnetization M_s is not attained even in the high magnetic field of 15 Oe. The same trend is observed for all the studied samples. The magnetization behavior obtained is a typical characteristic of nano-sized particles that are superparamagnetic at room temperature [35]. The values of saturation magnetization are estimated from the extrapolation of M vs. 1/H plot and listed in Table 4. From the table it is clear that the substitution of Ni^{2+} ions by Co^{2+} ions, which have a stronger preference for occupying the octahedral sites, increases the magnetic moment and consequently the net magnetization.

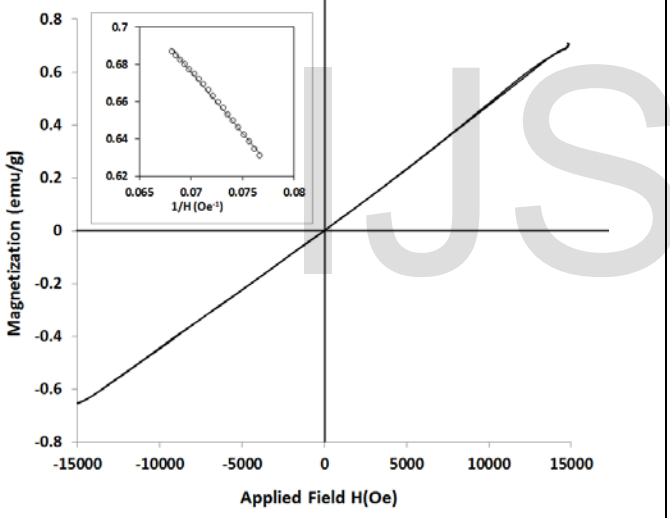

Fig. 6 Magnetization curve M-H of $CoAl_2O_4$ nano particles (C1.0).

The experimental magnetic moment η_{exp} is determined from the saturation magnetization data using the following formula [36]:

$$\eta_{exp} = MW * M_S / 5585 \qquad (8)$$

where η_{exp} is the magnetic moment of the samples expressed in Bohr magnetons (μ_B), MW is the molecular weight of the samples and M_S is the saturation magnetization in emu/g. The theoretical magnetic moments were also for both of tetrahedral η_A and octahedral η_B cationic sites calculated using the estimated cation distribution present in Table 3. Form which the net magnetic moments η_{th} [37] ($\eta_{th} = \eta_B - \eta_A$) were calculated and tabulated also in Table 3. It can be seen that, there is a good agreement between the experimental and calculated calculations for all the compositions except for $NiAl_2O_4$. This may be attributed to the presence of some NiO in the sample C0.0.

Table 3: Cation distribution, Saturation magnetization (M_S), and magnetic moment (η_{exp}, η_{th}) of $Ni_{1-x}Co_xAl_2O_4$ samples.

Sample	Cation distribution	M_S (emu/g)	$\eta_{exp}(\mu_B)$	$\eta_{th}(\mu_B)$
C0.0	$(Ni_{0.0104}Al_{0.9895})^A$ $[Ni_{0.9896}Al_{1.0104}]^B$	0.075	0.0023	1.9584
C0.2	$(Ni_{0.277}Co_{0.180}Al_{0.543})^A$ $[Ni_{0.523}Co_{0.020}Al_{1.457}]^B$	0.299	0.0094	0.0120
C0.4	$(Ni_{0.084}Co_{0.340}Al_{0.576})^A$ $[Ni_{0.516}Co_{0.06}Al_{1.424}]^B$	0.436	0.0130	0.0240
C0.6	$(Ni_{0.026}Co_{0.410}Al_{0.564})^A$ $[Ni_{0.374}Co_{0.19}Al_{1.436}]^B$	0.580	0.0180	0.0360
C0.8	$(Ni_{0.0101}Co_{0.453}Al_{0.5369})^A$ $[Ni_{0.1899}Co_{0.347}Al_{1.4631}]^B$	0.940	0.0290	0.0416
C1.0	$(Co_{0.48989}Al_{0.51011})^A$ $[Co_{0.5101}Al_{1.48989}]^B$	1.137	0.0360	0.0607

4. Conclusions

A series of Co substituted nickel aluminate (NPs) with an average size in the range of 3-27 nm were successfully synthesized by using a sol-gel auto combustion method. The crystal structures of all samples are cubic spinel. The estimated cation distribution which confirmed by XRD and VSM, indicate that the Ni, Co and Al ions are distributed over A– and B–site. The lattice parameters, crystallite size and saturation magnetization were found to increase by increasing the Co^{2+} content. Uv-Vis. spectra of (NPs) illustrate direct transition with an optical energy band gap in range of 3.1-3.6 eV. The substitution of Ni^{2+} ions by Co^{2+} ions point out to the formation of ceramic materials with blue color. Magnetic properties of (NPs) at room temperature reveal superparamagnetic behavior and remain unsaturated within the field 15 KOe. These results suggested that the Ni-Co aluminates (NPs) could be a promising candidate for biological applications and also can be employed to obtain ceramic blue pigments.

References

[1] X. Duan, D. Yuan, Z. Sun, C. Luan, D. Pan, D. Xu, M. Lv, (2005) J. Alloys Compd. 386:311.
[2] F. Pompeo, D. Gazzoli, N.N. Nichio (2009) Int. J. Hydrogen Energy 24:2260.
[3] H. Cui, M. Zayat, D. Levy (2005) J. Non-Cryst. Solids 351:
[4] D.M.A. Melo, J.D. Cunha, J.D.G. Fernandes, M.I. Bernardi, M.A.F Melo, A.E. Martinelli (2003), Mater. Res. Bull. 38:1559.
[5] J.J. Vijaya, L.J. Kennedy, G. Sekaran, M. Bayhan, M.A. William (2008) B, Chemical 134(2):604.
[6] D. Ding, W. Cai, M. Long, H. Wu and Y. Wu (2010) Solar Energy Materials and Solar Cells 94(10):1578.

[7] L. Torkian, M. Daghighi (2014) Advanced Powder Technology 25(2):739.
[8] Z. Chen, E. Shi, W. Li, Y. Zheng, N. Wu, W. Zhong (2002) J. Am. Ceram. Soc. 85: 2949.
[9] L.B. Kong, J. Ma, H. Huang (2002) Mater. Lett. 56: 238.
[10] M.K. Nazemi, S. Sheibani, F. Rashchi, V.M. Gonzalez-DelaCruz, Caballero A (2012) Advanced Powder Techn. 23:833.
[11] P.P. Phule, T.E. Wood (2008) Encyclopedia Mater.: Sci. Techn. 1090.
[12] A.R. Phani, M. Passacantando, Santucci S (2001) J. Mater. Chem. Phys. 68: 66.
[13] M.A. Laguna-Bercero, Sanjuán ML, Merino RI (2007), J. Phys. Condens . Matter. 19:1.
[14] J.W. Kim, P.W. Shin, M.J. Lee, S.J. Lee (2006) J. Ceram. Proc. Res. 7:117.
[15] J.N. Roelofsen, R.C. Peterson, M. Raudsepp (1992), Am. Mineralogist 77:522.
[16] R. Ianos, P. Barvinschi (2011) J. Eur. Ceram. Soc. 31: 739.
[17] X. Duan, M. Pan, F. Yu, D. Yuan (2011) J. Alloys Compd. 509:1079.
[18] CIE, Recommendations of Uniform Color Spaces, Color Difference Equations, Psychometrics Color Terms, Supplement no. 2 of CIE Publ. No. 15 (E1–1.31), (1971), Bureau Central de la CIE, Paris, (1978).
[19] Y.S. Han, J.B. Li, X.S. Ning, X.Z. Yang, Chi B (2004) Mater. Sci. Eng. A 369:241.
[20] B.D. Cullity, Elements of X-ray Diffraction (1956) Addison Wesley Pub. Co.Inc.
[21] B.D. Cullity, Elements of X-ray Diffraction (1978), Addison-Wesely, Reading, MA, USA.
[22] A.Yu Chapskaya , N.I. Radishevskaya, N.G. Kasatskii, O.K. Lepakova, Yu. S Naiborodenko, Vereshchagin VV (2005) J. Glass Ceram. 62: 11.
[23] L.F. Koroleva (Chekhomova) (2004) Glass Ceram. 61:299.
[24] Z. Chen, E. Shi, W. Li, Y. Zheng, W. Zhong (2002) Mater. Lett. 55:281.
[25] F. Meyer, R. Hempelmann, S. Mathur, M. Veith (1999) J. Mater. Chem. 9:1755.
[26] S. Brunauer, R. Sh. Mikhail, E. E. Bodor (1967), J. Colloid. Interface Sci. 24:451.
[27] M. Llusar, A. Fores, J.A. Badenes, J. Calbo, M.A. Tena, G. Monros (2001)J.Eur. Ceram. Soc. 21:1121.
[28] A.A. Verberckmoes, B.M. Weckhuysen, R.A. Schoonheydt (1998), Micropor. Mesopor. Mater. 22:165.
[29] F. Matteucci, G. Cruciani, M. Dondi, G. Gasparotto, D.M. Tobaldi (2007) J. Solid State Chem. 180: 3196.
[30] P. Jeevanandam, Yu. Koltypin, A. Gedanken (2002), Mater. Sci. Eng. B 90:125.
[31] C.F. Song, M.K. Lu, F. Gu, S.W. Liu, S.F. Wang, D. Xu, D.R. Yuan (2003) Inorg. Chem. Commun. 6:523.
[32] M. Jestl, I. Maran, A. Kock, W. Beinsting, E. Gornik (1989) Opt Lett 14:719.
[33] J. Schanda, Colorimetry: Understanding the CIE System (2007), New Jersey, Wiley, 61-64.
[34] S. Ibrahim, H. Shokrollahi, M.D. Mohammad, R. Safi (2012) J. Magnetism and Magn. Mater.324:1854.
[35] Jiaqi Wan, Xuehui Jiang, Hui Li and Kezheng Chen (2012) J. Mater. Chem. 22:13500.
[36] A. Pradeep, P. Priyadharsini, G. Chandrasekaran (2008) J. Magn. Magn. Mater. 320: 2774.
[37] W.F. Vander, G.A. Sawatzky, A.H. Morrish (1968) Phys. Rev. 167:533.